Journal Name

ARTICLE

Lewis Acidity Quantification and Catalytic Activity of Ti, Zr and Al-Supported Mesoporous Silica

M. V. Zakharova,[a] F. Kleitz*[b] and F.-G. Fontaine*[a]

[a] Département de Chimie, Centre de Catalyse et Chimie Verte (C3V), Université Laval, 1045 Avenue de la Médecine, Québec (Québec), Canada, G1V 0A6

[b] Département de Chimie, Centre de Recherche sur les Matériaux Avancés (CERMA), Université Laval, 1045 Avenue de la Médecine, Québec, QC G1V 0A6, Canada.

Email : frederic.fontaine@chm.ulaval.ca and freddy.kleitz@chm.ulaval.ca

Journal Name

ARTICLE

Lewis Acidity Quantification and Catalytic Activity of Ti, Zr and Al-Supported Mesoporous Silica

M. V. Zakharova,[a] F. Kleitz*[b] and F.-G. Fontaine*[a]

Water-tolerant supported Lewis acids are actively sought after, in particular to address the challenging direct amidation reaction. To this aim, a versatile and easy synthesis of large pore silica materials with supported Ti-, Al-, Zr- Lewis acids, using acetyl acetonate as metal-stabilizing agent, was accomplished. The formation of bulk metal oxides was not observed, even at high concentration of metal species. The Lewis acidity was demonstrated using quantitative and qualitative titration techniques using a series of Hammet indicators, such as butter yellow, phenylazodiphenylphosphine and dicinnamalacetone. The optimal concentration of metals corresponding to the highest Lewis acidity of solids was found to be 4% for Al-SBA-15, 12-15% for Ti-SBA-15 and 7% for Zr-SBA-15 materials. The water-tolerance of the supported metal centers was explored by a pyridine adsorption-FTIR study before and after water addition. The metalated materials were used as water-tolerant heterogeneous catalysts for the amidation of electron-poor and bulky amines such as substituted anilines and morpholine obtaining 59-99% yield of the corresponding amides.

Keywords: metalation • mesoporous materials • Lewis acids • amide synthesis • heterogeneous catalysis

Introduction

Lewis acid catalysts are playing a primary role in many industrial chemical processes. Although not inclusive, the list of organic transformations and rearrangements catalyzed by Lewis acid catalysts include notably the Mukaiyama-Aldol,[1] the Diels-Alder[2] and the Friedel–Crafts[3] reactions, which commonly result in formation of new C-C, C-N and C-O bonds. The typical Lewis acids used for these applications include soluble complexes of Ti^{4+}, Al^{3+}, Sn^{4+}, and Zr^{4+}. However, the removal of homogeneous catalysts in large scale processes can be costly and troublesome and heterogeneous catalysis presents itself as an alternative of choice. Although many Lewis acidic materials have been reported, most of these compounds exhibit significant moisture sensitivity.[4] Moreover, conventional Lewis acids require pretreatment in order to break any Lewis adducts occurring between the active sites and moisture, which can lead to the degradation of the catalysts. In addition, the high interest in green solvents for catalysis makes the synthesis of water-tolerant solid Lewis acids a target of great interest.[5] Zeolites are among the most important examples of heterogeneous catalysts comprising both Brønsted and Lewis acidic sites, originating from the aluminum atoms residing in the framework.[6] In the early 1980s, titanium silicalite-1 (TS-1) materials were shown to exhibit isolated Lewis acid sites in crystalline microporous materials without the presence of Brønsted acid sites.[7] However, these Lewis acid sites were hardly accessible for chemical transformations, such as for oxidation, because of the microporosity of the materials. In order to catalyze reactions with larger substrates, Ti^{4+} atoms were also introduced into the framework of 12-membered ring zeolites (Ti-Beta) and into ordered mesoporous silica matrices (e.g., Ti-MCM-41).[8] However, in some cases, a lower reactivity with respect to TS-1 was observed suggesting that the location of the Ti sites and the environment surrounding these sites were influencing the activity.[9]

Metal-organic frameworks (MOF) also exhibit catalytically relevant features similar to zeolites, including large internal surface areas and uniform pore and cavity sizes.[10] Some MOFs having Al[11], Cd[12],

[a.] M. Zakharova, Prof. Frédéric-Georges Fontaine
Département de Chimie, Centre de Catalyse et Chimie Verte (C3V)
Université Laval
1045 Avenue de la Médecine, Québec, QC G1V 0A6, Canada
E-mail: frederic.fontaine@chm.ulaval.ca
[b.] Prof. Freddy Kleitz
Département de Chimie, Centre de Recherche sur les Matériaux Avancés (CERMA)
Université Laval
1045 Avenue de la Médecine, Québec, QC G1V 0A6, Canada
E-mail: freddy.kleitz@chm.ulaval.ca

Cu[13], In[14], Mn[15], Sc[16,17] or Cr[18] nanoclusters have been shown to be very active Lewis acid catalysts. However, the low stability of these materials toward moisture, temperature, and some reactants, owing to the presence of organic linkers, especially in comparison to the stability of the covalent Si-O bonds in zeolites, is significantly limiting their industrial use.[19] Nevertheless, in the past few years, some new synthetic strategies have been developed in order to overcome the aforementioned drawbacks.[20]

One of the most convenient and cheap supports for Lewis acid catalysts has been silica-based mesoporous materials[21-30] owing to their high specific surface area and relatively large pore sizes compared to zeolitic materials and MOFs.[25,26] Moreover, materials synthesized with non-ionic triblock copolymers as templates, e.g., SBA-15 (Hexagonal 2-D)[31,32], SBA-16 (Cubic 3-D)[31,33,34] and KIT-6 (Cubic 3-D)[35], were found to exhibit enhanced stability (hydrothermal and mechanical), owing to their larger pore wall thickness compared to ionic surfactant-based MCM-41-type mesoporous silica[36-38].

Only few approaches were reported in order to introduce metal Lewis acidic character to mesoporous solid supports. Among them, the incorporation of metal precursors into the framework of mesoporous silica,[39] the synthesis of hybrid periodically-ordered mesoporous organosilica (PMO) materials[40] and direct surface grafting[41-43] resulted in highly catalytically active solid materials. PMO materials contain organic N, O, S- moieties that are incorporated into the mesoporous framework while metal Lewis acidic centers are anchored to the surface through covalent interactions. In this way, Polarz and coworkers performed the synthesis of a PMO containing Al[III] centers for the asymmetric carbonyl-ene reaction.[44] Chuah reported the synthesis of Zr-SBA-15 with Zr[4+] ions incorporated into a mesoporous framework, which confers to the material strong Lewis acidity, as well as incorporating weak Brønsted acidic sites, essential for the Prins reaction between pinene and paraformaldehyde.[39] Recently, the Tilley[45] and Kleitz groups studied the co-condensation[46] and post-synthesis grafting[47] of Ti^{4+} organometallic precursors in large pore SBA-15 silica. Using a similar strategy, Hara successfully used these Ti-SBA-15 materials for the Mukaiyama-aldol condensation of benzaldehyde with 1-trimethylsilyloxy-cyclohexene in water.[48] However, despite the aforementioned progress, there is still significant lack of diversity and in-depth study of solid-supported Lewis acids capable to catalyze various transformations in the presence of moisture, which slows down their development and application.

In particular, the direct amidation catalyzed by heterogeneous Lewis acids still represents an important challenge since many pharmaceutically and biologically important compounds are constituted of amide bonds as building blocks.[49-53] The catalytic synthesis of amides from readily available starting materials is a priority area for the pharmaceutical industry.[49,53] There have been a limited number of heterogeneous Lewis acid catalysts studied for direct amidation of electron-poor or hindered amines such as

aniline and morpholine.[53] Sasaki and Sugi reported calcium containing mesoporous aluminosilicate molecular sieves, having both Lewis and Bronsted acidic properties, which show interesting activity in the catalytic amidation of palmitic acid with N-hexadecylamine.[54] Sarvari and Sharghi described the treatment of amines with formic acid in the presence of ZnO under solvent-free conditions to generate the corresponding formamides in excellent yields.[55] Shimizu also reported a solid niobium oxide capable to act as a reusable, inexpensive Lewis acid catalyst for the amidation of substrates such as anilines and α-hydroxycarboxylic acids.[53] Additionally, multiple heterogeneous Bronsted acids were reported for such purpose.[56] In the present study, we aim to develop efficient solid Lewis acid catalysts for the direct amidation reaction. For this, we are reporting the synthesis of Ti-, Al-, Zr-SBA-15 materials made by a straightforward post-synthesis metalation methodology using acetylacetonate metal precursors. A qualitative and quantitative study of the Lewis acidity of these materials was performed to fully ascertain the nature and the distribution of the active sites. The water tolerance of these materials was proven by pyridine adsorption-FTIR studies comparing their properties with and without water. Finally, the materials were applied to the Lewis acid-catalyzed amidation of aniline and morpholine with undecanoic acid, obtaining high catalytic performance.

Experimental section

Characterization techniques

Low-angle X-ray diffraction (XRD) patterns were collected on a Rigaku Multiflex diffractometer using Cu K_α radiation (λ = 0.1541 nm). The XRD scanning was performed at 30 kV and 40 mA (1.2 kW), with steps of 0.01 and an acquisition time of 2 s. The reference patterns of the different single metal oxides were obtained from the Powder Diffraction File 2 (PDF-2) database licensed by the International Center for Diffraction Data (ICDD). The nitrogen adsorption-desorption isotherms were determined at -196 °C using an Autosorb-1 sorption analyzer. Prior to analysis, the samples were outgassed at 200 °C (for non-passivated materials) and at 80 °C (for passivated materials) for 12 h. The pore size distribution was obtained by the non-local density functional theory (NLDFT) method and calculated using the Autosorb-1 1.55 software, supplied by Quantachrome Instruments, USA. The NLDFT kernel selected considers sorption of N_2 on silica at -196 °C assuming a cylindrical pore geometry and the model of equilibrium isotherm based on the desorption branch and compared to value obtained from adsorption branch (using the model of metastable adsorption). Attenuated total reflectance infrared (ATR-IR) spectra were recorded using a Nicolet Magna 850 Fourier transform spectrometer equipped with a liquid nitrogen cooled narrow band MCT detector. Each spectrum was obtained from the acquisition of 128 scans at 4 cm^{-1} resolution from 4000 to 700 cm^{-1} using a Happ–Genzel apodization. Diffuse-reflectance UV–vis spectra were recorded using a Varian Cary 500 spectrophotometer equipped with a Praying Mantis accessory. A Spectralon reflectance standard

Journal Name

ARTICLE

was used as a reference. X-ray photoelectron spectroscopy (XPS) spectra were collected on a Kratos Axis-Ultra electron spectrometer (UK) using a monochromatic Al Kα X-ray source (Al k = 1486.6 eV) at a power of 300W and operated at a base pressure of 10^{-10} Torr. Charge compensation was performed using a low-energy electron beam perpendicular to the surface of the samples. Survey spectra used for determining the elemental composition were collected at pass energy of 160 eV. SEM images and EDX spectra were recorded using a JEOL JSM-840 instrument with an acceleration voltage of 15 kV. The samples were first dispersed on an aluminum stub and coated with Au/Pd film before analysis. Spectra were recorded using backscattered electrons (BSE) technique to increase the contrast between the transition metal oxide particles and the external surface of the metalated SBA-15. High-resolution TEM (HR-TEM) and EDX analyses were carried out on a Cs-corrected Titan G2 ETEM at an accelerating voltage of 300 kV. EDX elemental mapping images were obtained from a square area of 15*15 nm (100*100 pixels) with an acquisition time of 1 s. For TEM/EDX imaging, powder samples were dispersed in acetone and a few drops of the solution were placed on a holey carbon film coated 300 mesh copper grid. ^{13}C cross-polarization (CP/MAS), ^{29}Si and ^{27}Al magic-angle-spinning (MAS) nuclear magnetic resonance (NMR) analyses were carried out on a Bruker Advance 300 MHz spectrometer (Bruker Biospin Ltd, Milton, Canada) at 75.4 MHz for ^{13}C, 59.6 MHz for ^{29}Si and 78.172 MHz for ^{27}Al nuclei correspondingly. ^{29}Si MAS NMR spectra were recorded with a spin echo sequence to avoid instrument background with a recycle delay of 30 seconds in a 4 mm rotor spinning at 10 kHz. ^{13}C CP/MAS NMR spectra were recorded with a 4 mm MAS probe with a spinning rate of 10 kHz and contact time of 1 ms. Chemical shifts were referenced to tetramethylsilane (TMS, δ= 0.0 ppm) for ^{29}Si and adamantane (δ= 28.6 ppm) for ^{13}C NMR. Liquid NMR spectra were recorded on a Varian Inova NMR AS400 spectrometer at 400.00 MHz (^{1}H NMR).

Synthesis of SBA-15 material. Mesoporous silica SBA-15 was synthesized using amphiphilic block copolymer P123 (Sigma-Aldrich, MW = 5800) as a structure-directing agent and tetraethyl orthosilicate (TEOS) as a silica source.[46] In a typical synthesis, 10 g of P123 was dissolved in a mixed solution of distilled water (75 g) and HCl (2 M, 250 ml) at 35 °C during 2 hours. TEOS (21.5 g) was then added into the clear solution and the mixture was stirred at 35 °C for 20 h, followed by heating the solution at 100 °C for 24 h under static conditions. The resulting white precipitate was stirred in water (100 ml) containing few drops of concentrated HCl for 30 minutes, filtered off and washed with water (100 ml). Calcination of

the resulting silica at 550 °C for 5 h in air resulted in mesoporous silica SBA-15.

Metalation of SBA-15. Ti-, Al- and Zr-SBA-15 materials with different molar ratios were synthesized using a post-grafting method as reported earlier[46,47] with some modifications. In a typical synthesis, 6 g of P123 was dissolved in a mixed solution of distilled water (114 g) and HCl (37 wt%, 3.5 ml) at 35 °C for 2 hours. TEOS (21.5 g) was then added into the clear solution and the mixture was stirred at 35 °C for 20 h, followed by heating at 100 °C for 24 h under static conditions. The resulting suspension containing precipitated SBA-15 (5 g) was added to a mixture of distilled water (145 g) and ethanol (15 g) at room temperature. After the pH of the solution was adjusted to 10.0 with diluted ammonia, a mixture of ethanol (20 g), of the respective metal precursor (titanium *iso*-propoxide, zirconium butoxide or aluminum *iso*-propoxide) and acetyl acetone (AA) (AA/M = 3.15) was slowly added to the mixture at 15 °C and then stirred for 2 h. After filtration and washing with ethanol, the material was calcined at 550 °C for 5 h in air in order to immobilize the metal species on the silica surface. The resulting Ti^{4+}, Zr^{4+} and Al^{3+} deposited mesoporous silica samples with different metal contents were denoted as M-x-SBA-15 (M=Ti, Zr, Al; x = metal molar % obtained from XPS surface analysis). The silica yield is assumed to be 100 %. For comparison purposes, the materials were compared to bulk anatase TiO_2, ZrO_2 (Alfa Products) and γ-Al_2O_3 (Sigma-Aldrich) used without additional purification.

Passivation of SBA-15 and M-SBA-15. Passivation of surface silanol groups was performed using tetramethyldisilazane (TMDS) as a silylating agent.[57] In a typical protocol, 1 g of SBA-15 material preliminary degassed at 160 °C in a vacuum oven overnight was dispersed in 50 ml of dry hexanes and 2 ml of TMDS was added dropwise under vigorous stirring. The mixture was left stirring for 24 h at room temperature. The excess TMDS was removed by Soxhlet extraction for 12 h at 60 °C using dichloromethane as a solvent. The obtained passivated materials were then dried in a 60 °C oven for 12 h.

Investigation of the Lewis acidity

Titration of solids with Hammet indicators. The titration with Hammet indicators was performed accordingly to protocols described elsewhere.[58,59] Color tests were made by transferring about 0.1 g of dried and powdered solid to a test-tube, adding 3-5 ml of freshly distilled benzene, followed by the addition of a 0.1 % solution of the indicator in benzene (three drops). From the results

of such tests, it was easy to decide whether the solid under study was basic to all indicators, acid to all indicators, or had an H_0 value lying between two adjacent indicators. The samples were dried and stored in a screw-cap bottle in a desiccator prior to the colorimetric tests. The effect of water adsorption was to either decrease the color intensity of the absorbed indicators or to cause a shift to lower acid strengths. By carrying out parallel tests inside and outside a dry box, water adsorbed during a single transfer of dried sample to the test-tube had a negligible effect on acid strength.

Pyridine Adsorption FT-IR experiments. The adsorption tests were performed on 50 mg of solid materials freshly degassed at 160 °C for 24 h which were dispersed in 3 ml of a 5 % pyridine solution in dry hexane. After stirring the solid suspension for one hour, the solvent was removed under reduced pressure and the solids were continuously outgassed first at 100 °C for 1 h and then at room temperature for 16 h. As a final step, the white powders were analyzed by FT-IR spectroscopy.

Quantitative titration. The quantitative titration technique developed by Johnson[59] was modified so that the indicators could be added to portions of the metalated catalyst suspension after it had been equilibrated with *n*-butylamine.[60] Prior to the titration tests, 0.1 wt% solutions of the Hammet indicators in dry benzene were prepared and used the same day. About 600 mg of freshly calcined metalated materials were transferred to a 150 °C vacuum oven and dried for 24 h. About 200 mg of sample was transferred into dried 8 ml vials and 6 ml of dry benzene was added to each of the samples. Different volumes of a 0.1 M solution of *n*-butylamine in benzene were added to these samples (0.1, 0.2, 0.3 and 0.4 mmoles of *n*-butylamine per gram of powder). The tightly capped samples were then stirred vigorously at room temperature for 4 h (increasing the time to 12 h did not influence the titration test results). Each of the suspensions were separated in three different dry 8 ml vials (2 ml of a suspension containing approximately 67 mg of the catalyst) and 4 drops of one Hammet indicator solution were added, repeating the process for each indicator. The quantification of the number of acidic sites was done by considering the amount of *n*-butylamine required before no color change was observed with the Hammet indicator.

Catalytic amidation test. Passivated solid catalysts were degassed at 70 °C under reduced pressure in a vacuum oven for 24 h prior to the catalytic tests. In a typical experiment, the carboxylic acid (1 mmol), the amine (1 mmol) in toluene (2.5 mL) and the metalated SBA-15 (50 mg) were added to a round-bottom flask equipped with a reflux condenser and a magnetic stirrer. The reaction mixture was heated to reflux under an N_2 atmosphere and stirred for 48 h. After completion of the reaction, dichloromethane (25 ml) was added to the mixture, and the solid catalyst was separated by centrifugation followed by one cycle of washing with 25 ml of dichloromethane after which the centrifugation was repeated. After a second centrifugation, the organic fractions were combined and acidified with 5% aqueous HCl. The final product was extracted from the dichloromethane organic phase, dried over $MgSO_4$ and concentrated under a rotary evaporator. The yield of the product was determined by using ^{1}H NMR spectroscopy with dry 1,3,5-trimethoxybenzene as an internal standard.

Results and discussion

Materials characterization

Al-, Ti- and Zr-metalated materials were synthesized according to a modified post-synthesis protocol,[43,44,47] using acetyl acetonate as a metal-stabilizing agent to prevent the formation of metal oxide clusters in the pore channels or on the external surface of the solids. The presence of this ligand has been shown to reduce the rate of M-O-M formation while increasing the generation of M-O-Si linkages, thus favoring the formation of single metal sites and avoiding the generation of bulk metal oxides. Therefore, the use of such Ti, Al, and Zr precursors chemically modified with organic ligands resulted in high metal dispersion on the silica surface.[46,47] The Ti^{4+}, Zr^{4+} and Al^{3+} deposited mesoporous silica samples with different metal contents were denoted as M-x-SBA-15 (M=Ti, Zr, Al; x = metal molar % obtained from XPS surface analysis). The metal quantity was varied from 1 to 20 mol% in order to obtain the materials with high metal loading while preserving mesoporosity.

First of all, the synthesized materials were analyzed using nitrogen physisorption at -196 °C (Figure 1). Typical type IV isotherms with H1 hysteresis loops were identified for all materials with the exception of Zr-7%-SBA-15, where the uniformity of the mesopores was significantly lost upon the introduction of 10 mol% of zirconium-alkoxide precursors (Figure 1C). In the latter case, a broad pore size distribution was observed with a maximum at 9.3 nm (Table 1). Similar observations were done by other research groups when attempting to graft zirconium to SBA-15 materials, which was attributed to mesopore blocking caused by the formation of zirconia (ZrO_2 particles) inside the pores at higher loadings (above 10 mol%).[61-65,66]

For the Al-SBA-15 materials (Figure 1A) one can observe the onset of the capillary condensation step shifted to lower relative pressures when the concentration of the aluminum grafted on the surface increases. Similar effect was observed for Ti-SBA-15 (Figure 1B) and Zr-SBA-15 (Figure 1C) materials, but in the latter two classes of materials this effect was significantly less pronounced than in the case of the Al-containing mesoporous materials. In the case of low Ti, Al and Zr loadings, a higher volume of nitrogen was adsorbed compared to that of the parent SBA-15 (Table 1). Such phenomenon was reported for the impregnation of metals in a SBA-15 solid matrix, where an increase of up to 15 % of the total volume adsorbed and of the BET surface area were observed when compared to starting SBA-15 material.[68] Block polymer templated ordered mesoporous materials, such as SBA-15 silica, usually contain micropores/small mesopores, or at least a very rough channel surface, in their framework walls.[32] Loading the materials with Ti-, Al- and Zr-alkoxides can alter this microporous corona in a

Journal Name

ARTICLE

difficult-to-control manner and lead to some change in the sorption data at low metal loading. In particular, an increase in specific surface area and in the volume adsorbed seems possible, if restructuring of the microporous section of the walls takes place.[68]

X-ray photoelectron spectroscopy was used to probe the metal concentration on the surface.[46,47] As presented in Table 1, only a fraction of the initial metal-alkoxide concentration (4-20 mol%) can be grafted on the surface. Whereas the maximum concentration of metals in Al- and Ti-containing materials (respectively, 20 and 15 mol%) were obtained when the highest concentration of metallic starting materials was used (respectively, 50 and 40 mol%), a maximum loading of 7 mol% was observed for the Zr materials when a 10 mol% of zirconium alkoxide was used. A higher loading of 40 mol% of the zirconium starting reagent only led to 6% Zr incorporation, presumably caused by the formation of bulk zirconium oxide. The latter material was labeled as Zr-6%-SBA-15*. It is worth noting that the grafting of a 7 mol% concentration on silica materials without formation of crystalline zirconia was only observed once before.[67]
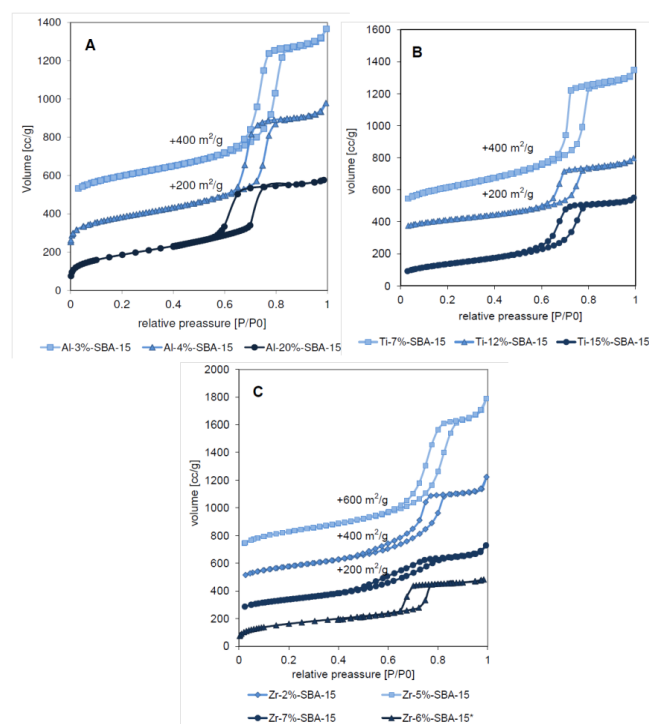

Table 1. Physicochemical properties derived from N_2 sorption measurements at -196 °C and XPS analysis performed on the different Ti-, Al- and Zr-SBA-15 materials.

Figure 1. N_2 adsorption–desorption isotherms measured at 77.4 K (-196 °C) for Al- (A), Ti- (B), Zr-SBA-15 (C).

Wide-angle powder X-ray diffractograms of metalated SBA-15 silica as well as the reference metal oxides are shown in Figure S2 (see Supporting Information). In all cases, except for Zr-6%-SBA-15*, no crystalline TiO_2, Al_2O_3 or ZrO_2 phase was identified on the surface indicating that either the metal layers coated on the pore walls were amorphous in nature and did not crystallize even after calcination at 550 °C or metallic particles were too small to be detected.**Erreur ! Signet non défini.** This suggests that the metal species are predominantly inside the pores of SBA-15 restricting the growth of crystals. Zr-6%-SBA-15* material exhibits broad signals at 30-33° and 50-60° that were attributed to the presence of ZrO_2 (Figure S2). Indeed, the SEM images of Zr-6%-SBA-15* materials reveal ZrO_2 particles outside the mesopores with an estimated size of 15 microns (Figure 2C). The elemental composition of zirconia particles was confirmed by EDX analysis and compared to the amorphous phase of Zr-grafted SBA-15 fragment (Figure 2D, E). The EDX spectrum of the particles appearing white (Figure 2C, ZrO_2) consists predominantly of those expected for ZrO_2, while spectra of the amorphous domain (Figure 2C, Zr-SiO_2) demonstrates three major signals for silica, oxygen and zirconium with a corresponding Si/Zr intensity of 6%. Besides Zr-6%-SBA-15*, the characteristic thread-like morphology of SBA-15 was observed for all materials and no crystalline domains were detected (Figure 2A, B).

The fact that Ti- and Al- metal oxide particles did not crystallize even at higher calcination temperatures suggests the presence of strong interactions of the grafted metals with the silica surface.[61,64] The presence of adsorption peaks at 940-990 cm^{-1} for Ti-SBA-15 materials using Fourier transform infrared (FTIR) spectroscopy of titanium-coated SBA-15 samples (Figure 3) indicates the existence of Si–O–Ti linkages, which are absent in the reference spectrum of bulk titania. Analogous observations were made for Al- and Zr-SBA-15 materials with corresponding M-O-Si stretching bands at 966 and 951 cm^{-1}, respectively (Figures S3-S4).

Sample	M/Si$_{initial}$ [mol%]	M/Si$_{final}$[a] [mol%]	S$_{BET}$[b] [m²/g]	NLDFT$_{ads}$[c] [nm]	NLDFT$_{des}$[d] [nm]	V$_t$[e] [cm³/g]
SBA-15	0	0	814	8.1	7.6	1.0
Ti-SBA-15						
1	10	7	777	8.8	9.1	1.4
2	30	12	408	8.1	8.1	0.7
3	40	15	472	8.1	8.1	0.8
Al-SBA-15						
4	4	3	721	9.3	9.7	1.4
5	10	4	671	9	9.2	1.4
6	50	20	403	7.3	7	0.5
Zr-SBA-15						
7	4	2	641	9.4	9.7	1.1
8	5	5	824	9.4	9.7/ 10.4	1.6
9	10	7	752	9.0	9.3$_{broad}$	1.3
10*	40	6	589	8.1	8.1	0.73

[a] Ti/Si molar ratio obtained by XPS technique; [b] S$_{BET}$, apparent BET specific surface areas deduced from the isotherm analyses in the relative pressure range from 0.05 to 0.20; [c] NLDFT$_{ads}$, primary mesopore diameter estimated using the NLDFT method. The model used for the NLDFT evaluation was N_2 adsorbed on silica with cylindrical pores assuming the adsorption branch (model of metastable adsorption); [d] NLDFT$_{des}$, primary mesopore diameter estimated using the NLDFT method. The model used for NLDFT evaluation was N_2 adsorbed on silica with cylindrical pores using the desorption branch (equilibrium sorption model); [e] V$_t$, total pore volume taken at relative pressure P/P$_0$=0.95.

The grafting of titanium to the surface increases the intensity ratio between the higher order reflections (110) and (200) and the (100) reflection. This phenomenon was documented earlier for rare-earth impregnated materials and attributed to the flattening of the electron density distribution inside the pores of the materials with low degree of metal surface.[68]

The low angle X-ray diffractograms of the titanated SBA-15 materials are shown in Figure S1 (see Supporting Information). The diffractograms show three diffraction peaks associated with the (100), (110) and (200) reflections at 0.91, 1.4 and 1.8° 2θ, indicating retention of the typical two-dimensional (2-D) hexagonal (symmetry group *p6mm*) structure of SBA-15.
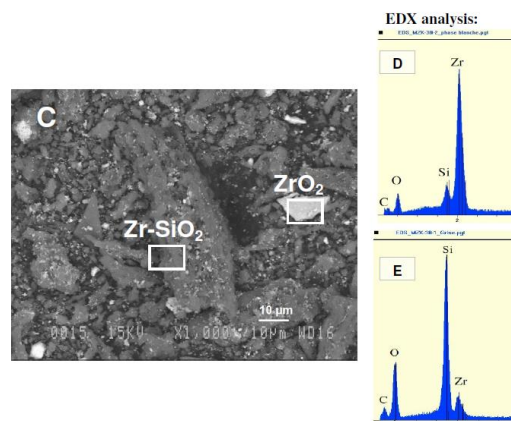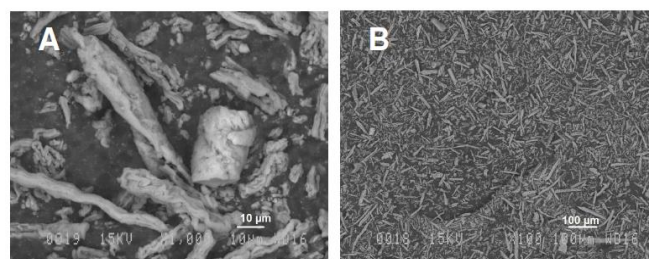

EDX analysis:

Journal Name

ARTICLE

Figure 2. SEM images of Ti-15%-SBA-15 material under x1000 (A) and x100 (B) folds magnification; SEM image of Zr-6%-SBA-15* under x1000 (C) fold magnification and EDX spectra Zr-6%-SBA-15* containing zirconia crystalline region (D) and amorphous region (E).

Figure. 4. UV-vis DR spectra of Ti-SBA-15 samples with different Ti concentrations.

Inspection of the UV-visible diffuse reflectance spectra (UV-vis DRS) of the titanium-coated SBA-15 samples gives a clear indication of the coordination environment of the metal centers (Figure 4). The materials having a low Ti loading on the material surface (such as Ti-7%-SBA-15) have a predominant signal between 250 and 260 nm, suggesting that titanium is essentially dispersed on the silica surface framework as TiO_4^{4-} tetrahedra.[46,47]
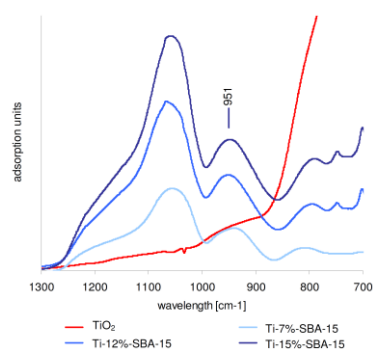

Figure 3. FTIR spectra of Ti-SBA-15 materials with different Ti concentrations.

However, when the titanium concentration increases up to 15%, a 45 nm red shift of the adsorption band to the 310-318 nm region was observed, probably due to the formation of some Ti–O–Ti bonds. This phenomenon was previously observed and attributed to formation of TiO_2 units in bulk amorphous titania.[46,47] Indeed, the reference bulk titania sample showed absorption bands at 250 and 280 nm caused by O^{2-} to Ti^{4+} charge-transfer in 4- and 6-coordinated TiO_2 species correspondingly.[46,47]
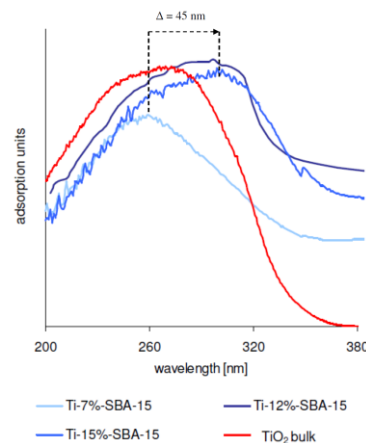
Solid state ^{27}Al MAS NMR was used as a complementary method for the determination of the coordination environment of the aluminum centers in the Al-SBA-15 materials. Similarly to Ti-SBA-15, both signals for the tetra- and hexa-coordinated metal species were observed with corresponding chemical shifts of 0 and 50-55 ppm.[69] A majority of tetra-coordinated centers are observed in low Al loadings, such as in Al-3%-SBA-15, whereas equal distributions of tetra- and hexacoordinated environments, with respective shifts of 0 and 51.3 ppm, were observed in Al-20%-SBA-15 (Figures S5-S7).

The high resolution transmission electron microscopy (TEM) analyses of Ti-SBA-15 materials are depicted in Figure 5A-F. These confirm the preservation of ordered mesopores after metalation. Also, no crystalline metal oxide was detected after the increase of titanium in the pores from 1 to 15 mol%. Energy-dispersive X-ray spectroscopy mapping reveals an even distribution of silicon, oxygen and titanium atoms as well as the gradual increase of titanium concentration without the formation of isolated domains. As it has been shown, using acetylacetonate as a stabilizing agent allows the successful grafting of Ti, Al and Zr on the surface of SBA-15 materials without formation of separated crystalline metal oxide domains, with the exception of the higher loadings of Zr.
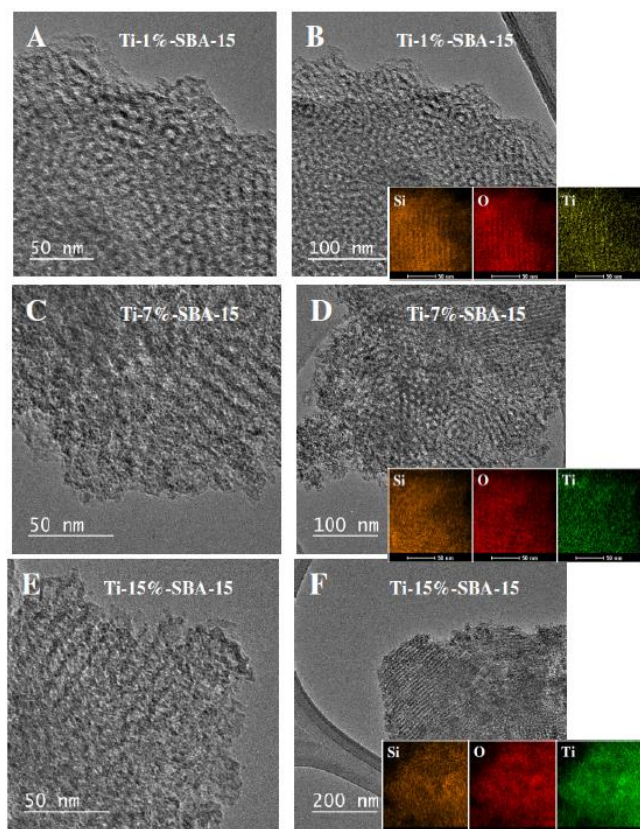
Figure 5. High resolution transmission electron microscopy spectra of Ti-SBA-15, where Ti 1% (A, B), Ti 7% (C, D), Ti 15% (E, F) and energy-dispersive X-ray spectroscopy data of Ti-SBA-15.

Surface acidity tests

In order to have a better insight into the surface acidity coming from the metal sites, colorimetric tests using various Hammet indicators were carried out. In order to apply the non-aqueous *n*-butylamine titration technique introduced by Benesi,[60] it has to be accepted that the pH scale used to determine the acid strength in dilute aqueous media can be extrapolated to very strong acidic media with corresponding negative values of pH. By the use of an appropriate series of indicators, the extrapolated pH scale can be given by H_o which is the Hammett acidity function (see Supporting Information for detailed information). Traditional methods of titration using Hammett indicators are widely used for measuring the acid strength of solid acids, superacids and ionic liquids.[61] Corma and Fornes used the Benesi method to quantify the amount of acidic centers as well as their strength in zeolites.[62] The mechanism of this titration consists in the interaction of a basic Hammet indicator (**B**) molecule with the surface Bronsted acidic sites (**HA**) or Lewis acidic sites (**LA**) with subsequent formation of the protonation product with the conjugated base (**HB⁺ + A⁻**) or of a Lewis pair adduct (**LA-B**), respectively. These products will be referred as the acidic forms of the Hammet indicators. Since these Hammet indicators are chromophores, such transformation is

accompanied by a dramatic color change of the solution due to a significant reorganization of the electronic structure. The colors of the acidic and basic forms of the Hammet indicators used in the present study, as well as their pK_a values, are presented in Table 2.

There is very little known about the acidity of metalated mesoporous materials. Xiao synthesized SiO_4^{2-}/ZrO_2 supported MCM-41 materials, which were later defined as solid superacids with H_0 values around −12.5, as determined using 2,4-dinitrotoluene as a Hammet indicator.[72] A pyridine adsorption-FT-IR study demonstrated these sites were Lewis acidic. Another interesting result was obtained by Antonelli and coworkers who developed a methodology for the synthesis of mesoporous materials containing Ti, Nb and Ta oxides.[73] The titration methods demonstrated that sulfated mesoporous Nb samples exhibited very strong acidity with $H_0 \leq -8.2$. In these materials, pyridine adsorption FT-IR analysis demonstrated that both Lewis and Bronsted acidic centers were present in a 50:50 proportion.[73]

Table 2. Hammet indicators used in the study, colors of the corresponding acidic and basic forms and their pK_a values.

Indicator	Acidic form	Basic form
Butter yellow (pK_a= +3.3)		
Phenylazodiphenylphosphine (pK_a= +1.5)		
Dicinnamalacetone (pK_a= -3)		

H_0 decreases, acidity increases →

The results of the titration of the Ti-, Al-, Zr-SBA-15 materials are presented in Table 3. It should be noted that the bulk metal oxides TiO_2, ZrO_2, Al_2O_3 and SBA-15, (Table 3, entries 1-4) did not induce color change. These results clearly demonstrate that grafting metal sites on the surface of SBA-15 material induces a very strong increase in acidity characterized by the change of color of the dicinnamalacetone indicator, suggesting a Hammet constant value lower than -3. Al-3%-SBA-15 (entry 5), Al-20%-SBA-15 (entry 7), Ti-4%-SBA-15 (entry 9), Ti-7%-SBA-15 (entry 10), Zr-2%-SBA-15 (entry 13) and Zr-6%-SBA-15* (entry 16) materials were able to partially change the color of dicinnamalacetone indicator; their Hammet constant was thus estimated to be within the range of [-1.5 - -3] units.

The optimal concentration of metal sites on the surface was found to be different according to the nature of the metal, as demonstrated by the color change of the Hammet indcator. It was shown that the optimal acidity was obtained when the materials comprised of 4% of Al, 12-15% of Ti or 5-7% of Zr. In the case of Al-SBA-15, an increase in the metal concentration did not have a significant influence on the acidity. In order to elucidate whether surface silanol groups of the silica support have an effect on the acidity of the metalated materials, passivated solids with optimal metal concentration were synthesized using tetramethyldisilazane

Journal Name

ARTICLE

(TMDS) as a protecting group[57] and their acidity was tested. After passivation of the surface silanol groups, the materials were able to produce a change of the color of all indicators, indicating that the surface metal centers are responsible for acidity (entries 17-21).

Table 3. Results of titration of Ti-, Al-, Zr-SBA-15 materials with Hammet indicators.

Entry	Sample	Butter yellow Acidic form	Butter yellow Basic form	Phenylazodiphenylphosphine Acidic form	Phenylazodiphenylphosphine Basic form	Dicinnamalacetone Acidic form	Dicinnamalacetone Basic form
1	SBA-15		yellow		yellow		yellow
2	Al₂O₃		yellow		yellow		yellow
3	TiO₂		yellow		yellow		yellow
4	ZrO₂		yellow		yellow		yellow
5	Al-3%-SBA-15	red		blue		purple	
6	Al-4%-SBA-15	red		blue		purple	
7	Al-20%-SBA-15	red		blue		purple	
8	Ti-1%-SBA-15	orange		light blue			yellow
9	Ti-4%-SBA-15	red		blue		light purple	
10	Ti-7%-SBA-15	red		blue		purple	
11	Ti-12%-SBA-15	red		blue		purple	
12	Ti-15%-SBA-15	red		blue		purple	
13	Zr-2%-SBA-15	red		blue		light purple	
14	Zr-5%-SBA-15	red		blue		purple	
15	Zr-7%-SBA-15	red		blue		purple	
16	Zr-6%-SBA-15*	red		blue		purple	
17	SBA-15-TMDS		yellow		yellow		yellow
18	Ti-12%-SBA-15-TMDS	red		light blue		light purple	
19	Ti-15%-SBA-15-TMDS	red		blue		light purple	
20	Al-4%-SBA-15-TMDS	red		blue		light purple	
21	Zr-7%-SBA-15-TMDS	red		blue		purple	

It is possible to distinguish between Lewis or Bronsted acidities by looking at the vibrational perturbations when a basic molecule (such as ammonia, pyridine or piperidine) is adsorbed on a solid surface, being a complementary tool to titration.[74] When pyridine interacts with surface Bronsted sites, the presence of the pyridinium species is evidenced by adsorption bands at 1540 and 1640 cm⁻¹, while the observation of bands at 1632-1580 and 1455-1438 cm⁻¹ are attributed to pyridine strongly adsorbed on Lewis acidic centers.[74] Deviations of several reciprocal centimeters can be observed according to the strength of the surface acidic centers. The water tolerance of the materials was tested by the addition of equimolar amounts of water. Figure 6 illustrates the spectra of pyridine adsorbed on the surface of Ti-, Al- and Zr-SBA-15 with variable concentrations. All the materials exhibit a significant majority of Lewis acidic centers compared to the Bronsted sites, even in presence of water. Zr-SBA-15 material demonstrated the strongest water-tolerant character, whereas the Ti- and Zr-SBA-15 materials produced small amount of Bronsted acidic centers upon the introduction of water into the system.
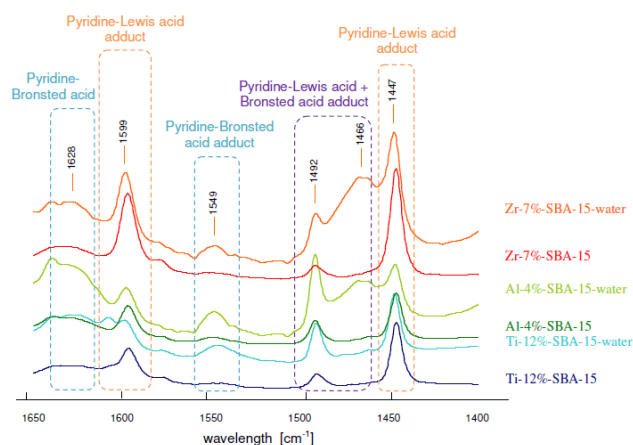

Figure 6. FT-IR spectra for pyridine adsorbed on Ti-, Al-, Zr-SBA-15 materials before and after water addition.

Once the Lewis acid character of the metalated solid was confirmed, a quantitative n-butylamine titration was performed. In Table 4, the amount of acidic sites for the selected materials is reported, which is determined by the amount of n-butylamine needed to prevent a color change of a selected Hammet indicator. Surface areas measured using the Brunauer-Emmett-Teller method (S_{BET}), as discussed earlier, allow the conversion of surface acid concentrations from a unit weight (mmol/g) to a unit surface (mmol/m²) basis. After comparing Lewis acidity of the obtained materials with initial metal loading, it becomes obvious that the Lewis acidity of the solid materials is not a function of the metal loading, but rather of the metal nature. Indeed, Al-4%-SBA-15 has a similar concentration of highly Lewis acid sites ($pk_a \leq -3$) than Ti-15%-SBA-15 (3.0 vs 3.8 mmol/m²) even if the metal loading in the latter material is four times higher. In the case of the Zr-7%-SBA-15, even if the concentration of acidic sites is the lowest of all materials, most of these sites are highly acidic, indicated by similar concentration of sites at $pk_a \leq +3.3$ and $pk_a \leq -3$ (1.3 vs 1.1 mmol/m²).

Table 4. Acidity of Al-, Ti-, Zr-SBA-15 materials

Material	S_{BET} [m²/g]	Sites with pk_a ≤+3.3		Sites with pk_a ≤+1.5		Sites with pk_a ≤-3	
		[mmol/g]	[mmol/m²] (x 10⁻⁴)	[mmol/g]	[mmol/m²] (x 10⁻⁴)	[mmol/g]	[mmol/m²] (x 10⁻⁴)
SBA-15	841	0	0	0	0	0	0
Al-4%-SBA-15	671	0.4	5.5	0.3	4.0	0.2	3.0
Ti-12%-SBA-15	408	0.25	6.1	0.2	4.7	0.1	2.5
Ti-15%-SBA-15	472	0.3	6.6	0.3	6.4	0.2	3.8
Zr-7%-SBA-15	752	0.1	1.3	0.1	1.2	0.1	1.1

Table 5. Catalytic amidation of aniline catalyzed by metalated SBA-15 materials.

Entry	Solid catalyst	Yield of amide [%]
1	-	1
2	SBA-15	40
3	SBA-15-TMDS	9
4	Al-4%-SBA-15	62
5	Al-4%-SBA-15-TMDS	61
6	Ti-12%-SBA-15	38
7	Ti-12%-SBA-15-TMDS	99
8	Zr-7%-SBA-15	26
9	Zr-7%-SBA-15-TMDS	76

Reaction conditions: aniline (96 mg, 1 mmol), undecanoic acid (184 mg, 1 mmol), solid catalyst (50 mg), dry toluene (3 ml), 110 °C, 48 h.

Catalytic amidation

The materials synthesized were tested as Lewis acids for the amidation of aniline with undecanoic acid. Conventionally, amides are synthesized from amines and activated carboxylic acid derivatives, such as carboxylic acid anhydrides or acyl chlorides, or through activation of a carboxylic acid with a stoichiometric amount of a condensation agent.[52,53] Therefore, the conventional methods suffer from the production of by-products. As such, it is generally accepted that the catalytic synthesis of amides from readily available starting materials is a priority area for the pharmaceutical industry.[49,53] Boron-[75,76] or transition metal-based[77] Lewis acidic homogenous catalysts have demonstrated several drawbacks such as water sensitivity, reduced activity by strong coordination of the basic functional groups, and difficulty in the removal of the catalyst. Some heterogeneous catalysts have been reported to effect the direct amidation, but these results were mainly limited to the N-formylation[52,78,79] or N-acetylation[52,80] of amines[53] and some of the systems require an excess of reagent.[81,82]

Aniline was chosen as a test-substrate for the direct amidation. The poor nucleophilicity of the nitrogen atom tends to lead to lower reactivity and requires a stronger activation of the carboxylic group for the catalysis to occur.[53] The results are presented in Table 5:
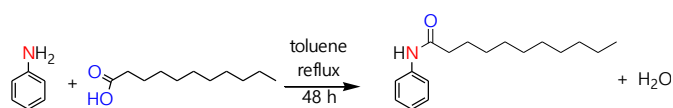
Without catalyst, the reaction does not proceed readily and only 1% of amide was obtained (entry 1). Quite interestingly, it was observed that pristine SBA-15 could provide the desired amide in 40% yield (entry 2). The ability of surface silanol groups to catalyze the amidation reaction was previously observed,[53] but the yield of the reaction is not constant and depends on the quality of the silica. The passivation of SBA-15 greatly reduces the catalytic activity, providing only 9% of the desired product under similar conditions (entry 3). The activity of the non-passivated and passivated materials was thus verified to compare the influence of the silanol groups on the activity. All materials were shown to catalyze the reaction, but Ti-12%-SBA-15-TMDS exhibited the highest catalytic activity with almost quantitative conversion (entry 7). The Zr-7%-SBA-15-TMDS material also exhibited significant catalytic activity with an isolated yield of 76%. Interestingly, lower yields were obtained for both the Ti- and the Zr-based non-passivated materials, obtaining 38 and 26% yields, respectively, suggesting that the presence of the silanol groups tend to reduce the influence of the Lewis acidity. It is possible that hydrogen bonding provided by the silanol groups on SBA-15 could limit the interaction of the carboxylic acid with the active metal centers or that the hydrophobic environment on the passivated materials would lead to a better exclusion of the water from the pores, which would lead to higher yields. However, no significant difference in

Journal Name

ARTICLE

isolated yields was observed when Al-4%-SBA-15 and Al-4%-SBA-15-TMDS materials were used (entries 4-5), giving 61-62% of the amide with both catalysts. Such observation is supported by the pyridine adsorption-FTIR experiments discussed earlier (Figure 6) and attributed to higher sensitivity of Al to water even after the passivation while Ti and Zr present stronger water tolerant Lewis acidic character and are thus less affected by the presence of water. Nevertheless, it should be noted that using wet solvents decrease slightly the yields observed in all cases.

Using Ti-12%-SBA-15-TMDS as a solid catalyst, we also tested the nature of the amine on the activity. The unsubstituted aniline was converted quantitatively (Fig. 7, A), but more electron rich 4-methoxyaniline gave only 29% yield (Fig. 7, B). Since the mass recovery with this sample was very low (about 55%), one can assume that the formation of Lewis adducts between the substrate and the catalyst reduces the catalytic activity. As such, electron-poor *para*-nitro- and *para*-fluoro-anilines give higher yields, obtaining 83% and 59%, respectively, of the amidation products (Fig. 7, C and D) with good mass recovery. Additionally, it was shown that the amidation of morpholine was also possible, obtaining 70% yield of the corresponding amide.
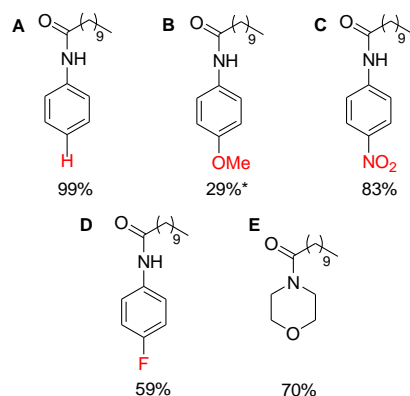

Figure 7. Reaction products with corresponding yields for substituted anilines (A-D), morpholine (E).

All the products of amidation reaction are new compounds, which were fully characterized (ESI). Unfortunately, despite the promising catalytic results, the material Ti-12%-SBA-15-TMDS exhibited significant loss in activity upon recycling of the material. It was observed that the yield of product **A** decreased from 99% to 56 and 16% after the second and third cycles, respectively. It is likely that Ti is either leaching or is deactivated upon catalysis. Further optimization of the catalysts to increase the reactivity and the reusability is currently ongoing.

Conclusions

In conclusion, a versatile and easy synthesis of Ti-, Al-, Zr-supported solid Lewis acids using acetyl acetonate as metal-stabilizing agent was demonstrated. It was shown that in most cases, no bulk metal oxide was formed during synthesis and that the metal distribution on the surface was achieved, even with 20 mol% of aluminum grafted on the surface. The Lewis acidity was explicitly substantiated by titration techniques with a series of Hammet indicators such as butter yellow, phenylazodiphenylphosphine, dicinnamalacetone. The water-tolerance of the supported metal centers was explored by means of pyridine adsorption-FTIR studies and compared before and after water addition. The optimal concentration of metal species, providing the highest acidity was identified and the dependence of metal the Lewis acidic element was shown. We demonstrated that metal species, supported on solid support through surface silanol groups are responsible for the strong Lewis acidity. We believe that such in-depth study provides an easy and systematic model of Lewis acidity characterization, which could be easily applicable to various solid materials. Finally, the metalated materials were shown to be exhibit some water tolerance for amidation of aromatic and bulky amines such as substituted anilines and morpholine. Although Ti-12%-SBA-15 still exhibits a limited recyclability, it is a highly active solid catalyst. This opens avenues for the use of such solid Lewis acids for the preparation of amide-containing compounds of pharmaceutical and biological interests.

Acknowledgements

References

1   T. Mukaiyama, *Angew. Chem., Int. Ed.,* 1977, **16**, 817-826.

2   E. J. Corey, *Angew. Chem., Int. Ed.,* 2002, **41**, 1650-1667.

3   M. Rueping and B. J. Nachtsheim, *Beilstein J. Org. Chem.,* 2010, **6**, 6.

4   A. Corma and H. García, *Chem. Rev.,* 2003, **103**, 4307-4365.

5   Y. Román-Leshkov and M. E. Davis, *ACS Catal.,* 2011, **1**, 1566-1580.

6   Selected articles: S. P. Sheu, H. G. Karge and R. Schlogl, *J. Catal.,* 1997, **168**, 278-291; K. Wang, X. Wang and G. Li, *Microporous Mesoporous Mater.,* 2006, **94**, 325-329; A. Aucejo, M. C. Burguet, A. A. Corma and V. Fornes, *Appl. Catal.,* 1986, **22**, 187-200; A. Jentys and J. A. Lercher, *Studies in Surface Science and Catalysis*, Elsevier Science B. V.: Amsterdam, 2001, Vol. 137; M. R. Basila, T. R. Kantner and K. H. Rhee, *J. Phys. Chem.,* 1964, **68**, 3197-3207; Z. S. Seddigi, *React. Kinet. Catal. Lett.,* 2001, **73**, 63-70; C. Costa, I. P. Dzikh, J. M. Lopes, F. Lemos and F. R. Ribeiro, *J. Mol. Catal. A: Chem.,* 2000, **154**, 193-201; L. Shirazi, E. Jamshidi and M. R. Ghasemi, *Cryst. Res. Technol.,* 2008, **43**, 1300-1306; J. Datka and E. *J.* Tuznik, *Catal.,* 1986, **102**, 43-51; P. L. Benito, A. G. Gayubo, A. T. Aguayo, M. Olazar and J. Bilbao, *J. Chem. Technol. Biotechnol.,* 1996, **66**, 183-191; C. Covarrubias, R. Quijada and R. Rojas, *Microporous Mesoporous Mater.,* 2009, **117**, 118-125; J. W. Ward, *J. Catal.,* 1970, **18**, 348-350; A. Rahman, G. Lemay, A. Adnot and S. Kaliaguine, *J. Catal.,* 1988, **112**, 453-463.

7   M. Taramasso, G. Perego and B. Notari, *US Patent*, 4, 410, 501, 1983; L. Shamleen, *KK US Patent*, 4, 623, 526, 1985; *US Patent*, 4, 519, 998, 1985; *European Patent*, B1, 0 148, 038, 1984; J. S. Reddy, R. Kumar and P. Ratnasamy, *Appl. Catal,* 1990, **58**, L1-L4; J. S. Reddy and R. Kumar, *J. Catal.* 1991, **130**, 440-446.

8   M. A. Camblor, A. Corma, P. Esteve, A. Martinez and S. Valencia, *Chem. Commun.*, 1997, 795-796.

9   W. Peng, Y. M. Liu, M. Y. He and T. Tatsumi, *J. Catal.,* 2004, 228, 183-191; A. Corma, M. T. Navarro and F. Rey, *Chem. Commun.*, 1998, 1899-1900; A. Corma, P. Esteve and A. Martinez, *J. Catal.,* 1996, **161**, 11-19.

10 D. Farrusseng, S. Aguado and C. Pinel, *Angew. Chem. Int. Ed.*, 2009, **48**, 7502-7513.

11 B. Li, K. Leng, Y. Zhang, J. J. Dynes, J. Wang, Y. Hu, D. Ma, Z. Shi, L. Zhu, D. Zhang, Y. Sun, M. Chrzanowski and S. Ma, *J. Am. Chem. Soc.*, 2015, **137**, 4243-4248; P. A. Wright, L. Mitchell, M. Clarke, V. R. Seymour, S. E. M. Ashbrook, P. Williamson, B. Ehrlichova, A. E. Anderson, N. Acerbi, L. Daniels and R. Walton, *Chem. Eur. J.,* 2014, **20**, 17185-17197.

12 M. Fujita, Y. J. Kwon, S. Washizu and K. Ogura *J. Am. Chem. Soc.*, 1994, **116**, 1151-1152.

13 K. Schlichte, T. Kratzke and S. Kaskel, *Microporous Mesoporous Mater.,* 2004, **73**, 81-88.

14 F. Gándara, B. Gomez-Lor, E. Gutiérrez-Puebla, M. Iglesias, M. A. Monge, D. M. Proserpio and N. Snejko, *Chem. Mater.*, 2008, **20**, 72-76.

15 S. Horike, M. Dinca, K. Tamaki and J. R. Long, *J. Am. Chem. Soc.*, 2008, **130**, 5854-5855.

16 F. Gándara, B. Gómez-Lor, M. Iglesias, N. Snejko, E. Gutiérrez-Puebla and A. Monge, *Chem. Commun.,* 2009, 2393-2395.

17 L. Mitchell, B. Gonzalez-Santiago, J. P. S. Mowat, M. E. Gunn, P. Williamson, N. Acerbi, M. L. Clarke and P. A. Wright *Catal. Sci. Technol.,* 2013, **3**, 606-617.

18 A. Henschel, K. Gedrich, R. Kraehnert and S. Kaskel, *Chem. Commun.,* 2008, 4192-4194.

19 Selected articles: J. Gascon, A. Corma, F. Kapteijn and F. X. Llabrés i Xamena, *ACS Catal.* 2014, **4**, 361-378; L. M. Huang, H. T. Wang, J. X. Chen, Z. B. Wang, J. Y. Sun, D. Y. Zhao and Y. S. Yan, *Microporous Mesoporous Mater.*, 2003, **58**, 105-114; S. Hausdorf, J. Wagler, R. Mossig and F. O. R. L. Mertens, *J. Phys.Chem. A,* 2008, **112**, 7567-7576; L. Alaerts, E. Seguin, H. Poelman, F. Thibault-Starzyk, P. A. Jacobs and D. E. De Vos, *Chem. Eur. J.,* 2006, **12**, 7353-7363; F. X. Llabrés i Xamena, A. Corma and H. Garcia, *J. Phys. Chem. C,* 2007, **111**, 80-85; *J. Catal.*, 2007, **250**, 294-298.

20 A. Corma, H. García and F. X. Llabrés i Xamena, *Chem. Rev.,* 2010, **110,** 4606-4655.

21 Q. Huo, D. I. Margolese, U. Ciesla, D. G. Demuth, P. Y. Feng, T. E. Gier, P. Sieger, A. Firouzi, B. F. Chmelka, F. Schuth and G. D. Stucky, *Chem. Mater.*, 1994, **6**, 1176-1191.

22 G. J. A. A. Soler-Illia, C. Sanchez, B. Lebeau and J. Patarin, *Chem. Rev.,* 2002, **102**, 4093-4138.

23 Y. Wan, Y. F. Shi and D. Zhao, *Chem. Commun.,* 2007, 897-926.

24 Y. Wan and D. Zhao, *Chem. Rev.,* 2007, **107**, 2821-2860.

25 T. Blasco, A. Corma, M. T. Navarro and J. P. Pariente, *J. Catal.,* 1995, **156**, 65-74.

26 M. Iglesias and F. Sánchez, *Catal. Lett.*, 1996, **39**, 153-156.

27 M. Morey, A. Davidson, H. Eckert and G.D. Stucky, *Chem. Mater.*, 1996, **8**, 486-492.

28 A. Corma, *Chem. Rev.*, 1997, **97**, 2373-2420.

29 Z. H. Luan, M. Hartmann, D. Zhao, W. Z. Zhou and L. Kevan, *Chem. Mater.*, 1999, **11**, 1621-1627.

30 Z.H. Luan, J.Y. Bae and L. Kevan, *Chem. Mater.*, 2000, **12**, 3202-3207.

31 D. Zhao, Q. Huo, J. Feng, B.F. Chmelka and G. D. Stucky, *J. Am. Chem. Soc.*, 1998, **120**, 6024-6036.

32 D. Zhao, J. Feng, Q. Huo, N. Melosh, G.H. Fredrickson, B.F. Chmelka and G.D. Stucky, *Science,* 1998, **279**, 548-552.

33 P. Van der Voort, M. Benjelloun and E. F. Vansant, *J. Phys. Chem. B,* 2002, **106**, 9027-9032.

34 T. W. Kim, R. Ryoo, M. Kruk, K. P. Gierszal, M. Jaroniec, S. Kamiya and O. Terasaki, *J. Phys.Chem. B,* 2004, **108**, 11480-11489; F. Kleitz, T. Czuryszkiewicz, L. A. Solovyov and M. Lindén, *Chem. Mater.,* 2006, **18**, 5070-5079.

35 T. W. Kim, F. Kleitz, B. Paul and R. Ryoo, *J. Am. Chem. Soc.*, 2005, **127**, 7601-7610.

36 A. Galarneau, D. Desplantier-Giscard, F. Di Renzo and F. Fajula, *Catal. Today* 2001, **68**, 191-200.

Journal Name

ARTICLE

37   A. Galarneau, M. F. Driole, C. Petitto, B. Chiche, B. Bonelli, M. Armandi, B. Onida, E. Garrone, F. Di Renzo and F. Fajula, *Microporous Mesoporous Mater*. 2005, **83**, 172-180.

38   K. Cassiers, T. Linssen, M. Mathieu, M. Benjelloun, K. Schrijnemakers, P. Van der Voort, P. Cool and E. F. Vansant, *Chem. Mater*., 2002, **14**, 2317-2324.

39   D. M. Do, S. Jaenicke and G.-K. Chuah, *Catal. Sci. Tech.,* 2012, **2**, 1417-1424.

40   U. Diaz, M. Boronat and A. Corma *Proc. R. Soc. London, Ser. A,* 2012, **468**, 1927-1954.

41   A. Vinu, P. Srinivasu, M. Miyahara and K. Ariga, *J. Phys. Chem. B,* 2006, **110**, 801-806; Y. Chen, Y. Huang, J. Xiu, X. Han and X. Bao, *Appl. Catal., A,* 2004, **273**, 185-191; A. Testino, I. R. Bellobono, V. Buscaglia, C. Canevali, M. D'Arienzo, S. Polizzi, R. Scotti and F. Morazzoni, *J. Am. Chem. Soc*., 2007, **129**, 3564-3575.

42   Z. Luan and J. A. Fournier *Microporous Mesoporous Mater.,* 2005, **79**, 235-240.

43   I. Jiménez-Morales, J. Santamaría-González, P Maireles-Torres and A. Jiménez-López *Appl. Catal. B*, 2011, **105**, 199-205; M. Gómez-Cazalillaa, J. M. Mérida-Roblesa, A. Gurbanib, E. Rodríguez-Castellóna and A. Jiménez-López, *J. Solid State Chem.,* 2007, **180**, 1130-1140.

44   A. Kuschel and S. Polarz, *J. Am. Chem. Soc*., 2010, **132**, 6558-6565.

45   J. Jarupatrakorn and T. D. Tilley, *J. Am. Chem. Soc*., 2002, **124**, 8380-8388; R. L. Brutchey, D. A. Ruddy, L. K. Andersen and T. D. Tilley, *Langmuir* , 2005, **21**, 9576-9583.

46   F. Bérubé, F. Kleitz and S. Kaliaguine *J. Phys. Chem. C,* 2008, **112**, 14403-14411.

47   T.-W. Kim, M.-J. Kim, F. Kleitz, M. M. Nair, R. Guillet-Nicolas, K.-E. Jeong, H.-J. Chae, C.-U. Kim and S.-Y. Jeong, *ChemCatChem,* 2012, **4**, 687-697; F. Bérubé, B. Nohair, F. Kleitz and S. Kaliaguine *Chem. Mater.,* 2010, **22**, 1988-2000.

48   N. K. Shintaku, K. Nakajima, M. Kitano, N. Ichikuni and M. Hara *ACS Catal*., 2014, **4**, 1198-1204.

49   D. J. C. Constable, P. J. Dunn, J. D. Hayler, G. R. Humphrey, J. J. L. Leazer, R. J. Linderman, K. Lorenz, J. Manley, B. A. Pearlman, A. Wells, A. Zaks and T. Y. Zhang, *Green Chem*., 2007, **9**, 411-420.

50   S. D. Roughley and A. M. Jordan, *J. Med. Chem*., 2011, **54**, 3451-3479.

51   J. S. Carey, D. Laffan, C. Thomson and M. T. Williams, *Org. Biomol. Chem*., 2006, **4**, 2337-2347.

52   E. Valeur and M. Bradley, *Chem. Soc. Rev*., 2009, **38**, 606-631.

53   M. A. Ali, S. M. A. H. Siddiki, W. Onodera, K. Kon and K. Shimizu, *ChemCatChem,* 2015, **7**, 3555-3561.

54   A. Sakthivel, K. Komura, S.-J. Huang, P.-H. Wu, S.-Bi. Liu, Y. Sasaki and Y. Sugi, *Ind. Eng. Chem. Res.,* 2010, **49**, 65-71.

55   M. Hosseini-Sarvari and H.Sharghi, *J. Org. Chem.,* 2006, **71**, 6652-6654.

56   J. W. Comerford, J. H. Clark, D. J. Macquarrie and S. W. Breeden, *Chem. Commun.*, 2009, 2562-2564; N. Narender, P. Srinivasu, S. J. Kulkarni and K. V. Raghavan, *Green Chem.,* 2000, 104-105; B.M. Choudary, V. Bhaskar, M. Lakshmi Kantam, K. Koteswara Rao and K.V. Raghavan, *Catal. Lett.,* 2001, 207-211; P. S. Chaudhari, S.D. Salim, R. V. Sawant and K. G. Akamanchi, *Green Chem.*, 2010, **12**, 1707-1710.

57   Y. Liang and A. Reiner, *J. Mater. Chem*., 2007, **17**, 2506-2516.

58   C. Walling, *J. Am. Chem. Soc*., 1950, **72**, 1164-1168.

59   O. Johnson, *J. Phys. Chem*., 1955, **59**, 827-831.

60   H. A. Benesi, *J. Phys. Chem.,* 1957, **61**, 970-973.

61   F. Schuth, A. Wingen and J. Sauer, *Microporous Mesoporous Mater*., 2001, **44–45**, 465-476.

62   W. Hua, Y. Yue and Z. Gao, *J. Mol. Catal. A: Chem*., 2001, **170**, 195-202.

63   M. V. Landau, L. Titleman, L. Vradman and P. Wilson, *Chem. Commun*., 2003, 594-595.

64   M. V. Landau, L. Vradman, X. Wang and L. Titleman, *Microporous Mesoporous Mater*., 2005, **78**, 117-129.

65   V. Degirmenci, O. F. Erdum, A. Yilmaz, D. Michel and D. Uner, *Catal. Lett*., 2007, **115**, 79-85.

66   L. Vradman, M. V. Landau, M. Herskowitz, V. Ezersky, M. Talianker, S. Nikitenko, Y. Koltypin and A. Gedanken, *J. Catal*., 2003, **213**, 163-175.

67   C. K. Krishnan, T. Hayashi and M. Ogura *Adv. Mater*., 2008, **20**, 2131-2136.

68   J. Sauer, F. Marlow, B. Spliethoff and F. Schüth, *Chem. Mater.,* 2002**, 14***,* 217-224.

69   V. Bosbeek, D. Freude, T. Frohlich, H. Pfeifer and H. Schmiedel, *J. Colloid Interface Sci*., 1982, **85**, 502-507; D. Freude, T. Frohlich, H. Pfeifer and G. Scheler, *Zeolites,* 1983, **3***,* 171-177.

70   M. Yurdakoç, M. Akçay, Y. Tonbul and K. Yurdakoç, *Turk. J. Chem*., 1999, **23**, 319-328; K. Tanebe, M. Misono, Y. Ono and H. Hattori, *New Solid Acids and Bases, Their Catalytic Properties, Studies in Surface Science and Catalysis*, Elsevier, Amsterdam, 1989, 51; K. Wang, X. Wang and G. Li, *Microporous Mesoporous Mater*., 2006, **94**, 325-329.

71   A. Aucejo, M. C. Burguet, A. A. Corma and V. Fornes, *Appl. Catal*., 1986, **22**, 187-200.

72   Y. Sun, L. Zhu, H. Lu, R. Wang, S. Lin, D. Jiang and F.-S. Xiao, *Appl. Catal. A,* 2002, **237**, 21-31.

73   Y. Rao and D. M. Antonelli, *J. Mater. Chem.,* 2009, **19**, 1937-1944.

74   T. Alemdaroglu, *Commun. Fac. Sci. Univ. Ank. Series B,* 2001, **47**, 27-35.

75   K. S. Ishihara, K. H. Ohara and K. Yamamoto, *J. Org. Chem.,* 1996, **61**, 4196-4197; T. Maki, K. Ishihara and H. Yamamoto, *Org. Lett*., 2006, **8**, 1431-1434; R. Yamashita, A. Sakakura and K. Ishihara, *Org. Lett.,* 2013, **15**, 3654-3657; N. Gernigon, R. M. Al-Zoubi and D. G. Hall, *J. Org. Chem*., 2012, **77**, 8386-8400; R. M. Al-Zoubi, O. Marion and D. G. Hall, *Angew. Chem. Int. Ed*., 2008, **47**, 2876-2879; R. M. Al-Zoubi, O. Marion and D. G. Hall, *Angew. Chem*., *Int. Ed*., 2008, **120**, 2918-2921; K. Arnold, A. S. Batsanov, Davies and B. A. Whiting, *Green Chem*., 2008, **10**, 124-134; E. K. W. Tam and L. Y. Liu, A. Chen, *Eur. J. Org. Chem*., 2015, 1100-1107; R. M. Lanigan, P. Starkov and T. D. Sheppard, *J. Org. Chem*., 2013, **78**, 4512-4523; D. C. Lenstra, F. P. J. T. Rutjes and J. Mecinović, *Chem. Commun*., 2014, **50**, 5763-5766.

76   T. Maki, K. Ishihara and H. Yamamoto, *Org. Lett*., 2005, **7**, 5043-5046.

77   Selected articles: H. Lundberg, F. Tinnis and H. Adolfsson, *Chem.-Eur. J*., 2012, **18**, 3822-3826; C. L. Allen, A. R. Chatwal and J. M. J. Williams, *Chem. Commun*., 2012, **48**, 666-668; F. Tinnis, H. Lundberg and H. Adolfsson, *Adv. Synth. Catal*., 2012, **354**, 2531-2536; *Synlett*, 2012, 2201-2204; A. C. Shekhar, A. R. Kumar, G. Sathaiah, V. L. Paul, M. Sridhar and P. S. Rao, *Tetrahedron Lett*., 2009, **50**, 7099-7101; Y. Terada, N. Ieda, K. Komura and Y. Sugi, *Synthesis,* 2008, 2318-2320; K. Steliou and M. A. Poupart, *J. Am. Chem. Soc*., 1983, **105**, 7130-7138.

78   H.-S. H. Sharghi, *J. Org. Chem*., 2006, **71**, 6652-6654.

79   V. K. Das, R. R. Devi, P. K. Raul, and A. Thakur, *Green Chem*., 2012, **14**, 847-854.

80   B. M. Choudary, V. Bhaskar, M. L. Kantam, K. K. Rao and K. V. Raghavan, *Catal. Lett*., 2001, **74**, 207-211.

81   E. Calcio Gaudino, D. Carnaroglio, M. A. G. Nunes, L. Schmidt, E. M. M. Flores, C. Deiana, Y. Sakhno, G. Martra and G. Cravotto, *Catal. Sci. Tech*., 2014, **4**, 1395-1399.

82   S. Nagarajan, P. Ran, P. Shanmugavelan, M. Sathishkumar, A. Ponnuswamy, K. S. Nahm and G. G. Kumar, *New J. Chem*., 2012, **36**, 1312-1319.